Electronic Supplementary Material (ESI) for ChemComm.
This journal is © The Royal Society of Chemistry 2016

Supporting Information for

Occurrence of Photoinduced Charge Separation by Modulating Electronic Coupling between Pyrene Dimer and Chemically Converted Graphene

Tomokazu Umeyama,*[a] Jinseok Baek,[a] Junya Mihara,[a] Nikolai V. Tkachenko,*[b] and Hiroshi Imahori*[ac]

[a] *Department of Molecular Engineering, Graduate School of Engineering, Kyoto University, Nishikyo-ku, Kyoto, 615-8510, Japan*

[b] *Department of Chemistry and Bioengineering, Tampere University of Technology, P.O. Box 541, FIN-33101 Tampere, Finland*

[c] *Institute for Integrated Cell-Material Sciences (WPI-iCeMS), Kyoto University, Nishikyo-ku, Kyoto 615-8510, Japan*

e-mail: umeyama@scl.kyoto-u.ac.jp, nikolai.tkachenko@tut.fi, imahori@scl.kyoto-u.ac.jp

Experimental

Instruments. NMR spectra were measured with a JEOL JNM-EX400 NMR spectrometer. Attenuated total reflectance (ATR) FT-IR spectra were recorded on a Themo Fisher Scientific Nicolet 6700 FT-IR. High-resolution mass spectra (HRMS) were obtained with a Thermo Fisher Scientific EXACTIVE. X-ray photoelectron spectroscopy (XPS) was carried out with ULVAC-PHI MT-5500 system with Mg Kα. Thermogravimetric analysis (TGA) measurements were conducted on a Shimadzu DTG-60H under a flowing N_2 gas at a scan rate of 2 ˚C min^{-1}. Resonance Raman spectra were measured using a Horiba Jobin Yvon LabRAM ARAMIS spectrometer equipped with an excitation wavelength of 633 nm (1.96 eV). Atomic force microscopy (AFM) analyses were carried out with an Asylum Technology MFP-3D-SA in the AC mode. CCG dispersions in DMF were spin-coated on freshly cleaved mica at 1000 rpm. The cross-section analyses of more than 55 sheets were conducted to estimate the average thicknesses. Transmission electron microscope (TEM) images were obtained from a JEOL JEM-2100F. For sample preparation, CCG dispersions in ethanol were dropped on microgrids (Cu mesh with carbon-supporting film) and dried under vacuum. UV-vis absorption spectra were measured with a Perkin-Elmer Lambda 900 UV/vis/NIR spectrometer. Steady-state fluorescence spectra were recorded on a HORIBA SPEX Fluoromax-3 spectrofluorometer. A time-correlated single photon counting (TCSPC) method was used for the fluorescence lifetime measurements in the nanosecond and subnanosecond time-scale and the time resolution was 310 ps (FWHM) for the excitation wavelength at 340 nm.[S1] Pump-probe measurements were carried out using the instrument described previously.[S2] Briefly, base 100 fs pulses were generated bu Libra F-1K (Coherent Inc.) which were utilized by OPO (Topas-C, Light Conversion Ltd.) to produce pump pulses at 430 nm, and probe white continuum in pump-probe detection system (ExciPro, CDP Inc.). A typical time resolution of the instrument was 150 fs (FWHM).

Materials. All solvents and chemicals were of reagent grade quality, purchased, and used without further purification. 4-(1-Pyrenyl)benzenediazonium tetrafluoroborate (Py-N_2BF_4),[S3] 1-(4-nitrophenyl)pyrene,[S3] 1,3,6,8-tetrakis(2,3,5,6-tetramethylphenyl)pyrene (MesPy-ref),[S4] surfactant

(sodium dodecyl sulfate (SDS))-wrapped chemically converted graphene (CCG),[S5] and iodophenyl-functionalized CCG (PhI-CCG)[S5] were prepared according to the reported procedures.

Synthesis

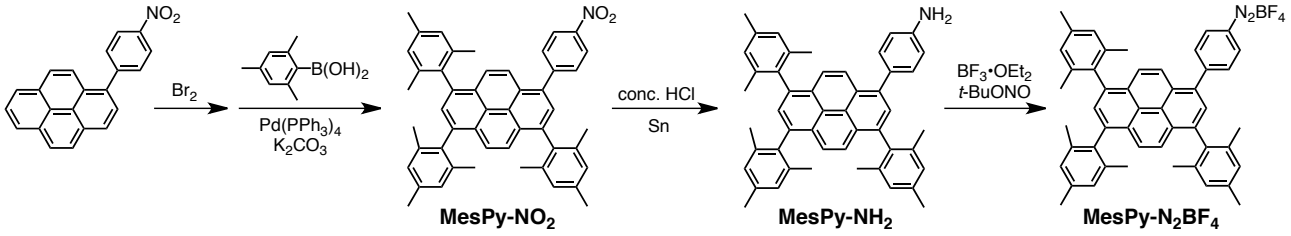

3,6,8-Trimesityl-1-(4-nitrophenyl)pyrene (MesPy-NO_2).[S6] Bromine (0.7 mL, 14 mmol) was added to a nitrobenzene solution (100 mL) of 1-(4-nitrophenyl)pyrene (1.3 g, 4 mmol). The reaction mixture was stirred at 120 ˚C for 18 h, then filtered and washed with ethanol to give crude 3,6,8-tribromo-1-(4-nitrophenyl)pyrene. A mixture of the crude product (1.1 g), 2,4,6-trimethylbenzeneboronic acid (2.0 g, 12 mmol), tetrakis(triphenylphosphine)palladium(0) (0.036 g, 0.33 mmol), and potassium carbonate (2.2 g, 16 mmol) in dry dioxane (20 mL) was stirred under nitrogen for 96 h at 110 ˚C. The reaction mixture was washed with water and then dried over $MgSO_4$. The solvent was evaporated under reduced pressure. Purification of the crude product by column chromatography (CH_2Cl_2/hexane, 1/2) afforded a yellow solid of MesPy-NO_2 (1.4 g, 95 %). ^{1}H NMR ($CDCl_3$, 400MHz): δ 8.37 (d, 2H, J = 8.7 Hz), 8.03 (d, 1H, J = 9.8 Hz), 7.81 (d, 2H, J = 8.6 Hz), 7.78, (s, 1H), 7.69 (d, 1H, J = 9.8 Hz), 7.65 (s, 1H), 7.58 (d, 1H, J = 9.8 Hz), 7.53 (d, 1H, J = 9.3 Hz), 7.04 (s, 2H), 7.03 (s, 2H), 6.99 (s, 2H), 2.40 (s, 1H), 2.39 (s, 1H), 2.38 (s, 1H), 1.95 (s, 2H), 1.94 (s, 2H), 1.92 (s, 2H). ATR-IR : ν_{max}/cm^{-1} 2962, 2915, 2850, 1596, 1520, 1476, 1456, 1377, 1344, 1012, 983, 854, 833, 816, 702, 605. HRMS (ESI): calcd for $C_{49}H_{43}NO_2$ 677.3288, found 677.3263.

3,6,8-Trimesityl-1-(4-aminophenyl)pyrene (MesPy-NH_2). To MesPy-NO_2 (1.1 g, 1.6 mmol) in ethanol/water (4 : 1, 85 mL) were added an excess of tin metal (1.8 g, 15 mmol) and concentrated hydrochloric acid (5 mL). The mixture was refluxed, and more acid was periodically added. After l

h, the reaction mixture was cooled to room temperature. The precipitated salts and residue from the evaporated solution were washed with water followed by dichloromethane, and then dried in air. The product was recovered as the hydrochloride salt. Powdered crystals of the salt of MesPy-NH_2 were added to dichloromethane in a separatory funnel followed by 20% aqueous sodium hydroxide. The mixture was shaken for 15 min until most of the solid had dissolved. The dichloromethane solution was separated, extracted again with aqueous sodium hydroxide, drawn off through a plug of glass wool in the stem of the separatory funnel, and dried over sodium sulfate. The solution was evaporated to become viscous oil, which slowly crystallized. Purification of the crude product by column chromatography (CH_2Cl_2) afforded a light green solid of MesPy-NH_2 (560 mg, 55 %). ^{1}H NMR ($CDCl_3$, 400MHz): δ 8.22 (d, 1H, J = 9.2 Hz), 7.78 (s, 1H), 7.61 (d, 1H, J = 9.2 Hz), 7.59 (s, 1H), 7.49 (s, 2H), 7.44 (d, 2H, J = 8.3 Hz), 7.04 (s, 2H), 7.02 (s, 2H), 7.00 (s, 2H), 6.82 (d, 2H, J = 8.3 Hz), 2.40 (s, 1H), 2.39 (s, 1H), 2.37 (s, 1H), 1.96 (s, 2H), 1.94 (s, 2H), 1.92 (s, 2H). ATR-IR : ν_{max}/cm^{-1} 3476, 3379, 2949, 2917, 2855, 1620, 1505, 1478, 1459, 1377, 1281, 1180, 1005, 905, 850, 837, 736, 615. HRMS (ESI): calcd for $C_{49}H_{45}N$ 647.3547, found 647.3531.

4-[1-(3,6,8-Trimesityl)pyrenyl]]benzenediazonium tetrafluoroborate (MesPy-N_2BF_4). To a round-bottom flask charged with a solution of $BF_3{\cdot}OEt_2$ (290 mL, 2.3 mmol) in DME (5 mL) was slowly added a solution of MesPy-NH_2 (1.0 g, 1.5 mmol) in DME (15 mL) with good agitation at −5 ˚C. Then *t*-BuONO (298 mL, 2.3 mmol) was added via syringe dropwise over at least 30 min. Precipitate formed during the addition. The reaction mixture was stirred at −5 ˚C in a brine/ice bath for 1h after the *t*-BuONO addition was completed. The reaction mixture was stirred and the brine/ice bath was allowed to warm to 0 ˚C. The reaction mixture was concentrated under reduced pressure. Then, the solid was dissolved in CH_2Cl_2, reprecipitated with diethylether, and filtered. Vacuum drying of the solid to a constant weight gave MesPy-N_2BF_4 (1.1 g, 98 %). ^{1}H NMR (CD_3OD, 400MHz): δ 8.76 (d, 2H, J = 8.8 Hz), 8.31 (d, 2H, J = 8.8 Hz), 8.07 (d, 1H, J = 9.3 Hz), 7.85 (s, 1H), 7.73 (d, 1H, J = 9.3 Hz), 7.63 - 7.53 (m, 3H), 7.08 (s, 2H), 7.07 (s, 2H), 7.05 (s, 2H), 2.40 (s, 1H), 2.38 (s, 1H), 2.37 (s, 1H), 1.93 (s, 2H), 1.92 (s, 2H), 1.91 (s, 2H). ATR-IR ν_{max}/cm^{-1}

3102, 2975, 2917, 2850, 2270, 1612, 1575, 1462, 1377, 1080, 906, 851, 755, 614.

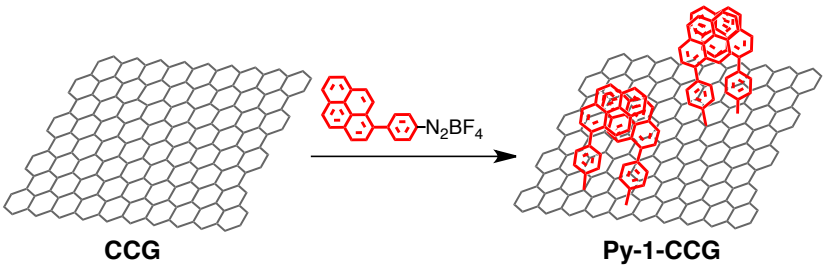

Py-1-CCG. Py-N_2BF_4 (2.5 g, 6.3 mmol) was added to the SDS-wrapped CCG dispersed in water (1 mg mL^{-1} based on CCG, 25 mL). The reaction mixture was stirred for 1 h at room temperature, and then poured into acetone to precipitate black powder. After filtration through a PTFE membrane with an average pore size of 200 nm, the black precipitate was washed with water and acetone to remove SDS and excess diazonium salt. The black powder was dispersed in DMF, and then filtered and washed thoroughly with DMF on the PTFE membrane. The resulting solid was dispersed in DMF, yielding Py-1-CCG dispersion. Py-1-CCG was stored in the dispersion state since the removal of the solvent by filtration yielded the black paper of Py-1-CCG that was difficult to re-disperse.

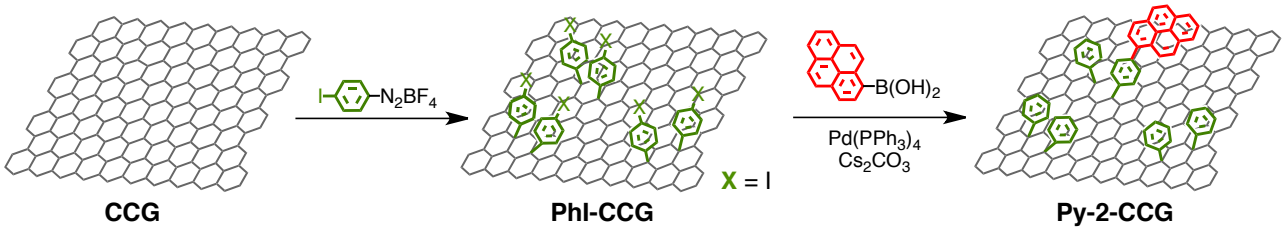

Py-2-CCG. PhI-CCG was prepared by the aryl addition reaction between 4-iodobenzenediazonium tetrafluoroborate and SDS-wapped CCG as described in a previous report.[S5] The preparation of Py-2-CCG was conducted as follows. After sonication of PhI-CCG dispersion in DMF (1 mg mL^{-1} based on PhI-CCG, 20 mL) for 10 min at room temperature, Cs_2CO_3 (0.8 g, 2.5 mmol) and 1-pyreneboronic acid (99 mg, 0.4 mmol) were added. This mixture was then degassed via three cycles of freeze-pump-thaw and refilled with argon. $Pd(PPh_3)_4$ (30 mg) was added and the reaction mixture

was stirred for 24 h at 100 °C under argon atmosphere. After cooling to room temperature, the mixture was diluted with THF (200 mL), sonicated for 5 min, and filtered through a PTFE membrane. The product was washed thoroughly with THF, methanol, water, methanol, and THF to remove excess pyrene. The resulting black cake was suspended in DMF, and then filtered and washed with DMF. The resulting solid was dispersed again in DMF, yielding Py-2-CCG dispersion. Py-2-CCG was stored in the dispersion state since the removal of the solvent by filtration yielded the black paper of Py-2-CCG that was difficult to re-disperse.

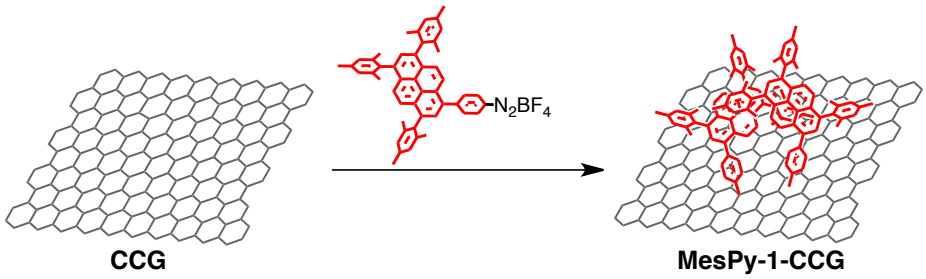

MesPy-1-CCG. MesPy-N_2BF_4 (1.1 g, 1.5 mmol) was added to the SDS-wrapped dispersion of CCG (5 mg). The reaction mixture was stirred for 1 h at room temperature, and then poured into acetone to precipitate black powder. After filtration through a PTFE membrane with an average pore size of 200 nm, the black precipitate was washed with water and acetone to remove SDS and excess diazonium salt. The black powder was dispersed in DMF, and then filtered and washed thoroughly with DMF on the PTFE membrane. The resulting solid was dispersed in DMF, yielding MesPy-1-CCG dispersion. MesPy-1-CCG was stored in the dispersion state since the removal of the solvent by filtration yielded the black paper of MesPy-1-CCG that was difficult to re-disperse.

Supporting discussion on functionalization ratios of Py-1-CCG, Py-2-CCG, and PhI-CCG

The degrees of pyrene functionalizations in Py-1-CCG and Py-2-CCG were estimated by comparing the integrated values of absorbance of the CCG and pyrene moieties in the region of frequencies at 14000 – 33000 cm^{-1} (300 – 600 nm, Fig. 2a), assuming that the integrated values of molar absorption coefficients of the pyrene moieties for Py-ref, Py-1-CCG, and Py-2-CCG and those of the CCG moieties for PhI-CCG, Py-1-CCG, and Py-2-CCG are identical.[S7] One 4-(1-

pyrenyl)phenyl (PP) unit is estimated to be attached per approximately 67 carbon atoms of CCG in Py-1-CCG, corresponding to one PP pair at approximately 1.7 × 1.7 nm^2 of one side of the CCG surface. Meanwhile, one PP unit is calculated to appear at the approximately 310 carbon atom point of CCG in Py-2-CCG, corresponding to one PP at approximately 3.6 × 3.6 nm^2 of one side of the CCG surface. To further characterize the functionalization, thermogravimetric analyses (TGA) of Py-1-CCG and Py-2-CCG were performed under an argon atmosphere (Fig. S2). However, the thermal decomposition profiles of Py-1-CCG and Py-2-CCG exhibited structureless decreases with no pronounced steps despite the sharp weight loss of Py-ref at < 280 ˚C. During thermal treatments under inert atmospheres, the defects in the graphene sheets of Py-1-CCG and Py-2-CCG may be healed by the attached pyrene units. Such a healing process was also observed in the porphyrin–CCG covalently linked system through the phenylene spacer.[S5]

X-ray photoelectron spectroscopy (XPS) measurement of PhI-CCG revealed that the ratio of C/I was 46, corresponding to a one PhI group per approximately 40 carbon atoms of CCG (Fig. S1a).[S5] Meanwhile, PhI-CCG showed weight loss in the temperature range from 300 to 450 ˚C, which reflects the detachment of covalently linked PhI groups (Fig. S2). From the difference in weight loss between CCG with no substituents and PhI-CCG, the degree of the functionalization is estimated to be one PhI per approximately 60 carbons of CCG. This functionalization ratio is lower than that estimated using XPS. The existence of residual PhI at > 450 ˚C may have caused the underestimation of the functionalization ratio by the TGA method. Then, Suzuki coupling reaction of PhI-CCG with pyrenyl boronic ester gave the pyrene-tethered CCG (Py-2-CCG). After the reaction, iodine signals totally disappeared in XPS (Fig. S1b). UV-vis absorption measurements, however, revealed a functionalization ratio of one PP group in ca. 310 carbon atoms of CCG (vide supra). Thus, the reaction yield of the Suzuki coupling on the SWNT sidewall was as low as ca. 15%. The rest of the iodine atoms in the PhI groups were consumed by an incomplete Suzuki coupling reaction.

Supporting discussion on absorption spectra in oxidized and reduced conditions

First, to judge whether the charge separation occurred or not with the photoexcitation of Py-2-CCG, the characterizations of the absorption spectra for the oxidized/reduced PP and CCG moieties are necessary. Therefore, we observed the changes in the absorption spectra of Py-ref and PhI-CCG under oxidized/reduced conditions.

The electrochemically oxidized Py-ref shows a positive absorption at < 550 nm and no signals in the near infrared (NIR) region (Fig. S11). Meanwhile, the electrochemically reduced PhI-CCG reveals a V-shaped positive absorption profile in the visible and NIR regions (Fig. S12b).[S8] Therefore, the second TA component of Py-2-CCG that shows negative absorption signal in the NIR region cannot be reconstructed with the sum of the spectra for the oxidized PP and the reduced CCG, which show no and positive absorption signals in the NIR region, respectively. These results exclude the possibility of the electron transfer (ET) from the excited PP group to the conduction band of CCG (Fig. S10a).

On the other hand, M. R. Wasielewski et al. reported the vis-NIR absorption spectrum of electrochemically reduced Py-ref, which showed broad absorptions at 400 – 650 nm and 650 – 1000 nm.[S9] Meanwhile, the electrochemical oxidation treatments of PhI-CCG led to undesired formation of the aggregates, preventing the absorption measurement of the oxidized CCG moiety. Instead, we conducted the chemical oxidation of PhI-CCG using $FeCl_3$ as an oxidant and measured the differential vis-NIR absorption spectrum (Fig. S12a). The oxidized PhI-CCG exhibits positive absorptions in visible and NIR regions with a negative peak at 620 nm. Thus, the spectrum shape of the second component of Py-2-CCG that shows negative absorption signal in the NIR region does not match with the sum of the spectra for the reduced PP[S9] and the oxidized CCG (Fig. S12a), both of which exhibit positive absorption bands in the NIR region. These results rule out the possibility of the ET from the valence band of CCG to the excited PP group (Fig. S10b).

Then, to judge whether the charge separation occurred or not with the photoexcitation of Py-1-CCG, the characterizations of the absorption spectra for the oxidized and reduced pyrene dimer moiety are also necessary. However, a model compound of the pyrene dimer was virtually unprocurable. Thus, we observed the changes in the absorption spectrum of Py-1-CCG under

oxidized and reduced conditions to extract the characteristics of the absorption spectra for the oxidized and reduced pyrene dimer.

The electrochemical oxidation treatments of Py-1-CCG led to undesired formation of the aggregates, preventing the absorption measurement of the oxidized pyrene dimer moiety. Instead, we implemented the chemical oxidation of Py-1-CCG using $Cu(OSO_2CF_3)_2$ as an oxidant and measured the differential vis-NIR absorption spectrum (Fig. S14a). When adding 0.028 μmol of $Cu(OSO_2CF_3)_2$ to 0.147 mg of Py-1-CCG in DMF (3 mL), the spectrum shows a positive absorption in visible and NIR regions with a negative peak at 620 nm (Fig. S14a, (i)), which is analogous to the oxidized PhI-CCG (Fig. S12a). Due to the higher energy level of the valence band of the functionalized CCG than the first oxidation potential of the pyrene dimer (Fig. S15a), the CCG moiety was oxidized in advance of the pyrene dimer. Subsequently, when adding 0.14 μmol of the oxidant to the dispersion of Py-1-CCG in DMF, the shape of spectrum significantly changed from that of the oxidized PhI-CCG; a broad positive absorption in visible and NIR regions with a positive peak at 680 nm (Fig. S14a, (ii)). This absorption spectrum may correspond to the sum of the spectra for the oxidized CCG and pyrene dimer, and thereby we subtracted the spectrum (i) from the spectrum (ii) in Fig. S14a to extract the characteristics of the absorption spectrum of the oxidized pyrene dimer. The differential spectrum shows a positive absorption at 540 – 900 nm with a peak at 650 nm and a bleaching at < 540 nm (Fig. S14a, (iii)). The shape of the spectrum is closely similar to that of the oxidized pyrene dimer on the SWNT sidewall in Py-1-SWNT,[S3b] corroborating that the differential spectrum (iii) in Fig. S14a represents the absorption spectrum of the oxidized pyrene dimer on CCG. Meanwhile, the electrochemically reduced PhI-CCG reveals a V-shaped positive absorption profile in the visible and NIR regions (Fig. S12b). Therefore, the third TA component of Py-1-CCG (Fig. 3a) can be reconstructed with the sum of the spectra for the oxidized pyrene dimer (Fig. S14a, (iii)) and the reduced CCG (Fig. S12b), exemplifying the formation of the complete CS state, i.e., the oxidized pyrene dimer and the reduced CCG, initiated by the photoexcitation of the pyrene dimer in Py-1-CCG.

On the other hand, spectroelectrochemical measurements of Py-1-CCG were performed under

the reducing conditions to extract the characteristics of the absorption spectrum of the reduced pyrene dimer. When applying –1.0 V vs. $Ag/AgNO_3$, the spectrum shows a broad positive absorption in the visible and NIR regions (Fig. S14b, (i)), which corresponds to the absorption spectrum of the reduced CCG moiety (Fig. S12b). Subsequently, when applying –3.0 V vs. $Ag/AgNO_3$, the spectrum exhibits relatively intense absorption bands in the visible region with a peak and a shoulder at 600 and 780 nm, respectively (Fig. S14b, (ii)). The differential spectrum obtained by the subtraction of spectrum (i) from the spectrum (ii) corresponds to the absorption spectrum of the reduced pyrene dimer (Fig. S15b), which clearly shows the bimodal absorptions in the visible region with a peak at 600 nm and a shoulder around 780 nm (Fig. S14b, (iii)). This bimodal absorption feature of the reduced pyrene dimer hinders the reconstruction of the third TA component of Py-1-CCG (Fig. 3a) by summing the spectra for the oxidized CCG (Fig. S12a) and the reduced pyrene dimer (Fig. S14b, (iii)), ruling out the possibility of the ET from the valence band of CCG to the excited PP dimer.

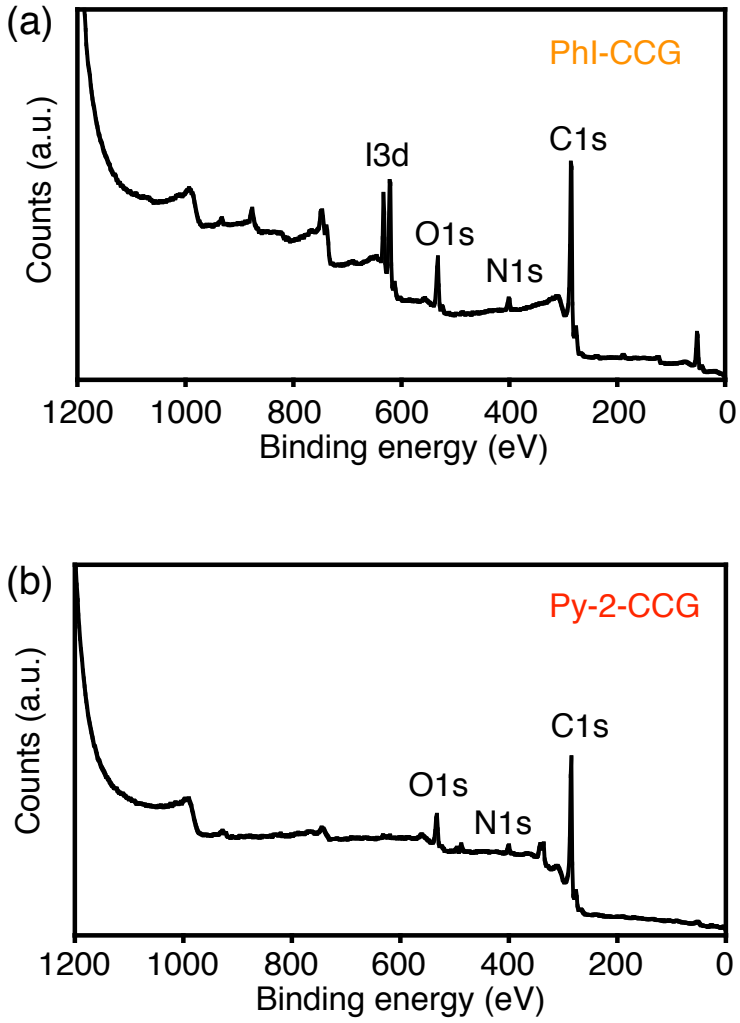

Fig. S1 XPS survey scans of (a) PhI-CCG and (b) Py-2-CCG. The ratio of C/I was estimated to be 46 in (a), corresponding to the functionalization ratio of one iodophenyl group per approximately 40 carbon atoms of CCG.

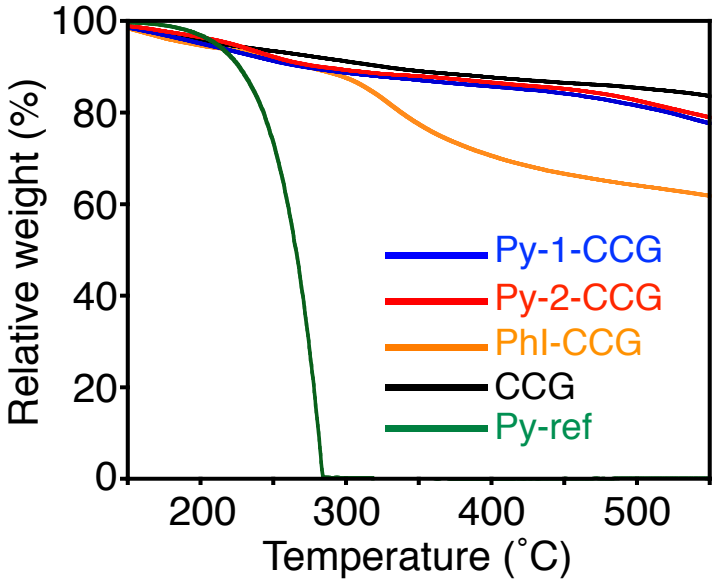

Fig. S2 Thermogravimetric analyses of Py-1-CCG (blue), Py-2-CCG (red), PhI-CCG (orange), CCG with no substituents (black), and Py-ref (green). The analyses were performed under nitrogen with a heating rate of 2 ˚C min^{-1}.

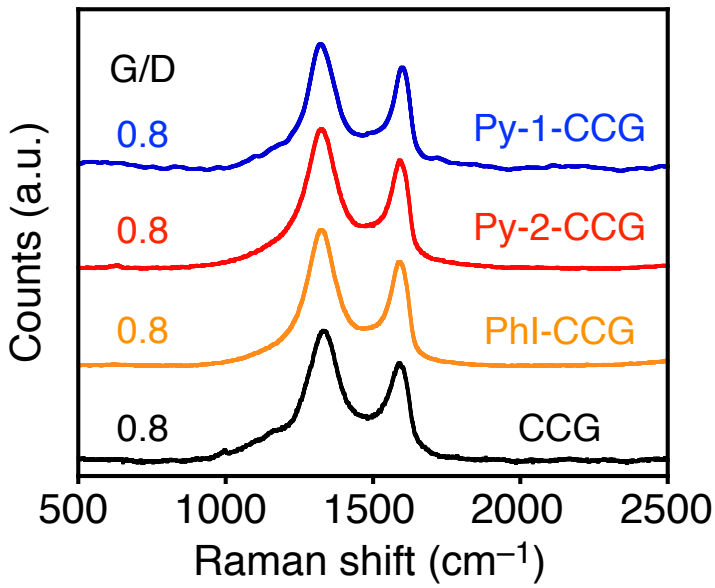

Fig. S3 Resonant Raman spectra of Py-1-CCG (blue), Py-2-CCG (red), PhI-CCG (orange), and CCG with no substituents (black) excited at 633 nm. The relative peak intensities of tangential mode (G-band) around 1580 cm^{-1} and of disorder mode (D-band) around 1340 cm^{-1} (G/D ratio) are also shown. The G/D ratio of CCG is 0.8, suggesting the incomplete recovery of a pristine graphene structure from GO. After the functionalization by the aryl addition reaction, the G/D ratio is still similar to that of CCG. Therefore, Raman spectroscopy does not allow us to estimate the functionalization degree. Tour et al. reported similar results for the preparation of CCG and its functionalizations using diazonium salts.[S10]

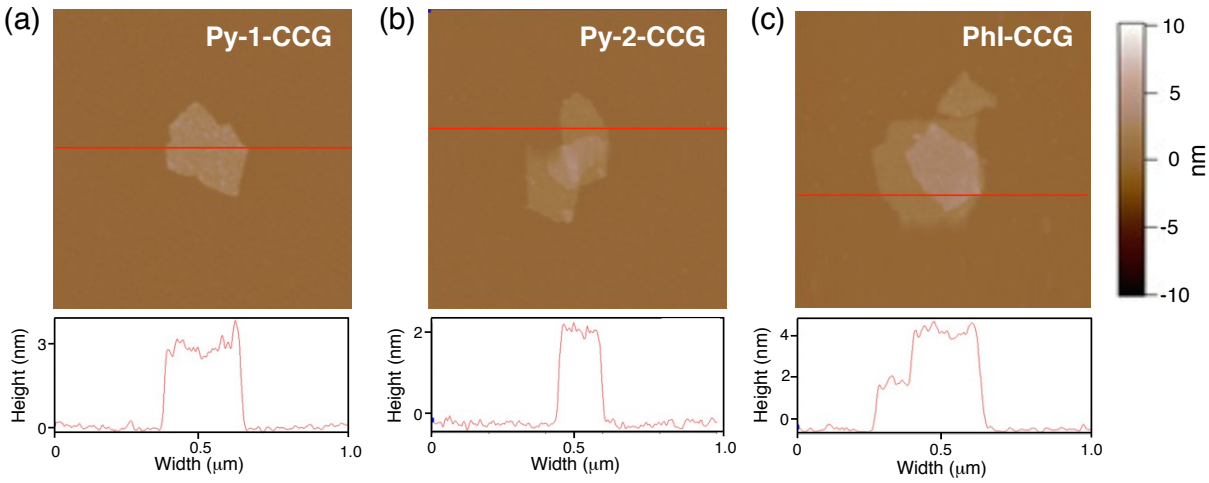

Fig. S4 AFM images with section profiles of (a) Py-1-CCG, (b) Py-2-CCG, and (c) PhI-CCG spin coated on a mica from the DMF dispersion. The color scale represents the height topography, with light and dark representing the highest and lowest features, respectively.

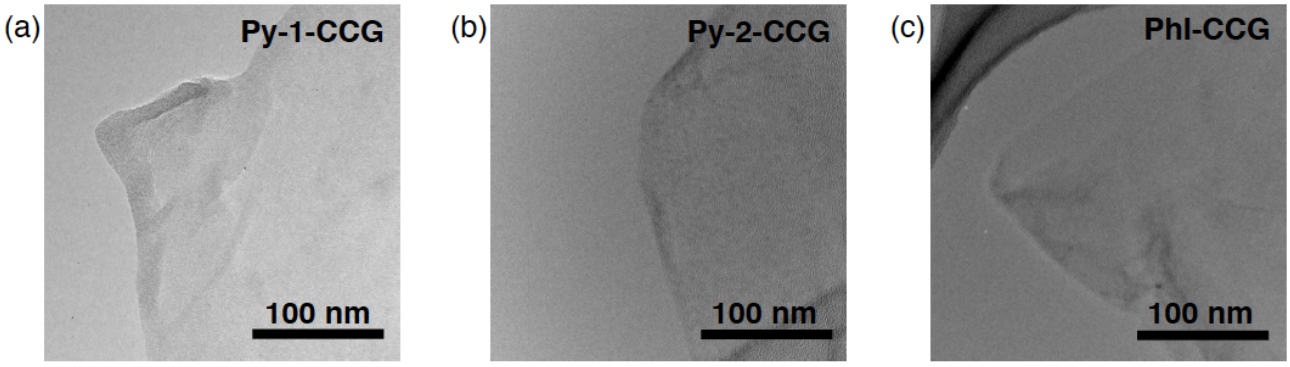

Fig. S5 TEM images of (a) Py-1-CCG, (b) Py-2-CCG, and (c) PhI-CCG. The samples were prepared by casting the ethanol dispersion onto a microgrid. Single-layered sheets with wrinkled edges in some parts are visible. The darker black parts in (c) are carbon-support films. The pyrenes fixed on the 2D basal plane of CCG are not visible owing to the complete overlap of the pyrenes and CCG in the projection image of TEM. This is in sharp contrast with successful visualization of the pyrenes grafted onto the sidewall of SWNTs as the ideal scaffold possessing highly curved 1D sp^2 carbon nanostructures for the TEM imaging.[S3b]

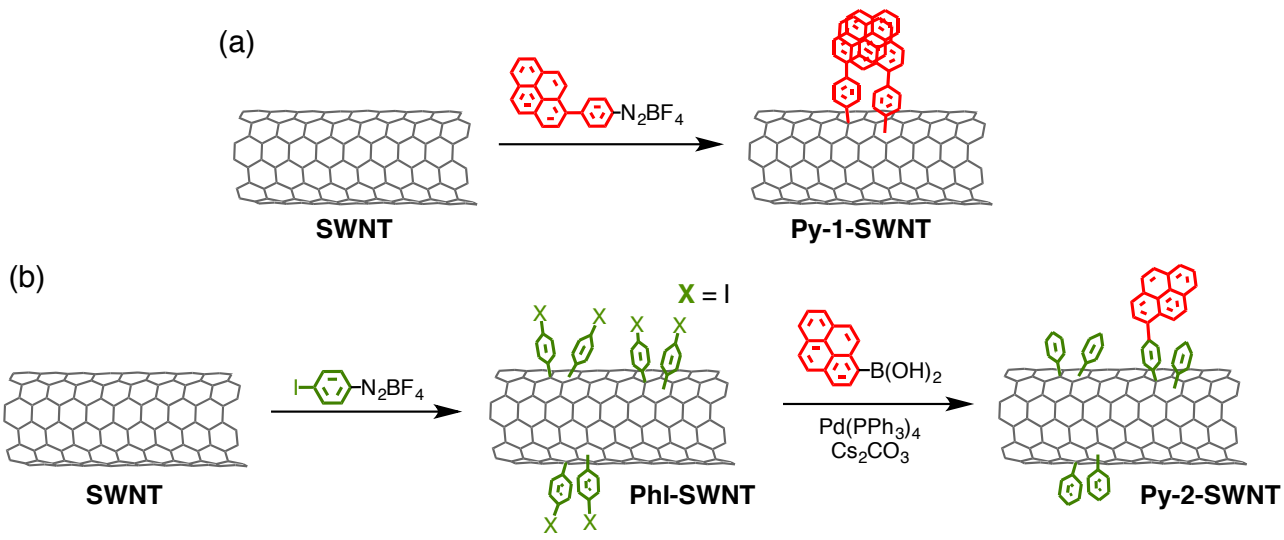

Fig. S6 Synthesis of (a) Py-1-SWNT and (b) Py-2-SWNT.

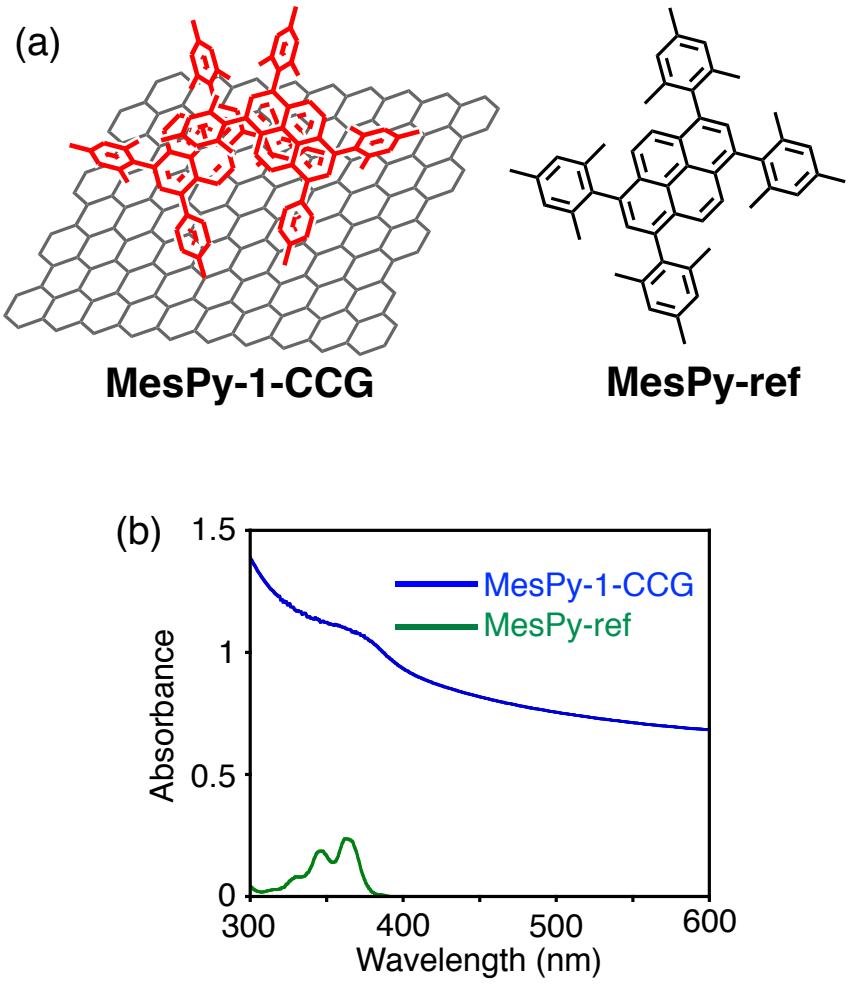

Fig. S7 (a) Structures of MesPy-1-CCG and MesPy-ref. (b) UV-visible absorption spectra of MesPy-1-CCG (blue) and MesPy-ref (green, 2.9 μM) in DMF. The degree of functionalization is estimated to be one MesPy unit per ca. 2200 carbon atoms of CCG in MesPy-1-CCG.

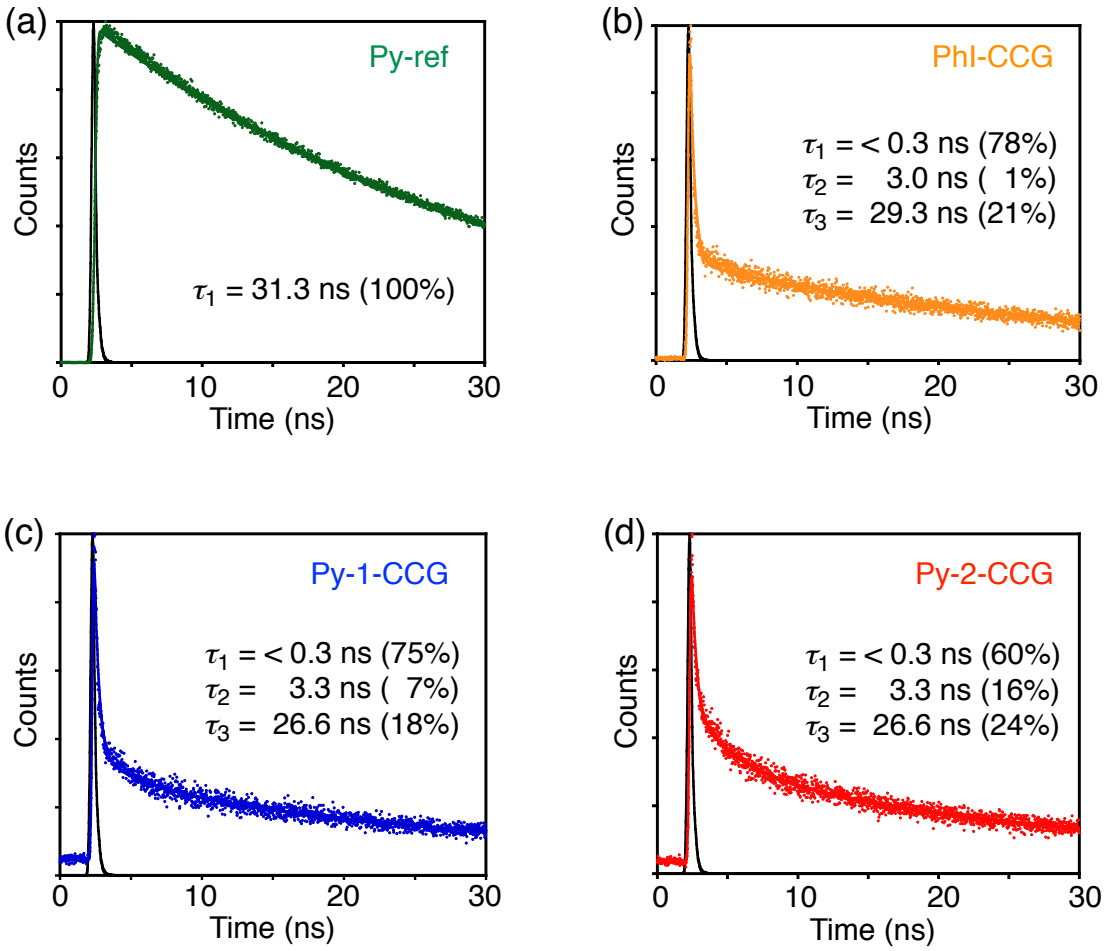

Fig. S8 Fluorescence decays of (a) Py-ref, (b) PhI-CCG, (c) Py-1-CCG, and (d) Py-2-CCG. The excitation and monitoring wavelengths are 340 and 390 nm, respectively. Note that both the pyrene and CCG are excited at 340 nm. The solid lines present decay fittings and the black lines show the instrumental response function. The fluorescence lifetimes with the ratios are given in the figures. Because the fluorescence decay profiles of Py-1-CCG and Py-2-CCG are similar to that of PhI-CCG, all three components in the fluorescence decays of Py-1-CCG and Py-2-CCG can be reasonably attributed to the excited CCG.

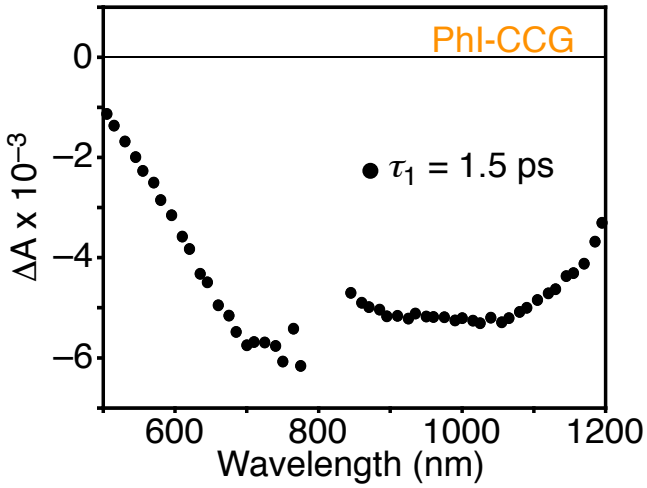

Fig. S9 Time-resolved transient absorption component spectrum of PhI-CCG in DMF obtained with global one-component fit of the data. The excitation wavelength is 350 nm. The lifetime of respective components is given in the figure.

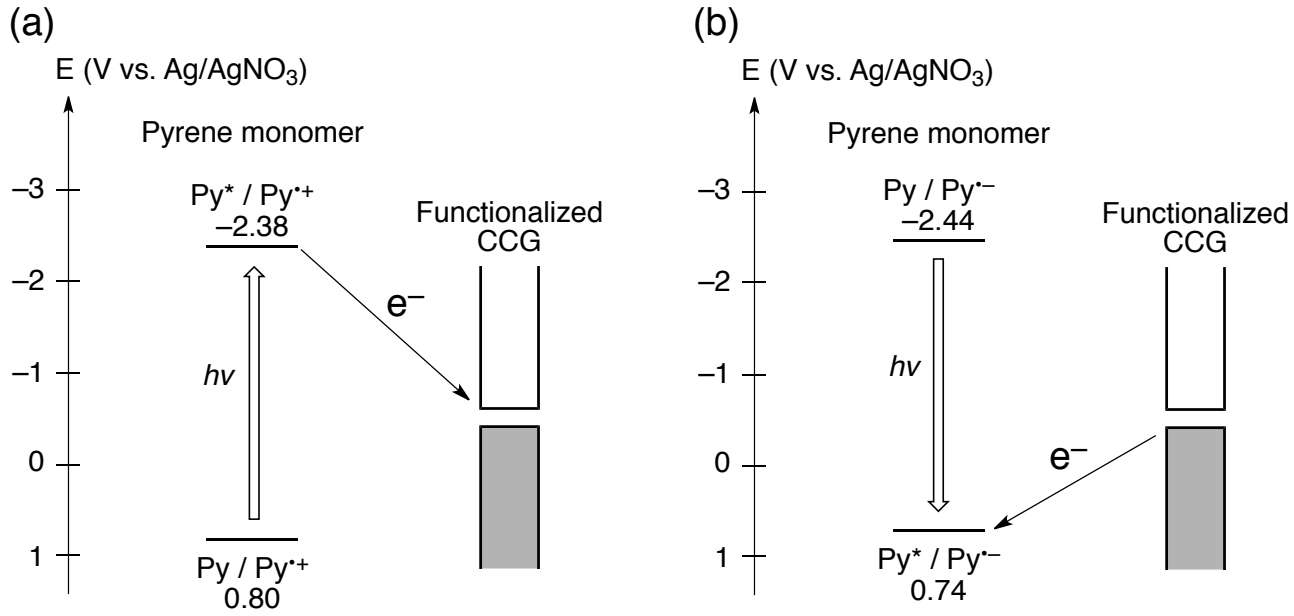

Fig. S10 Energy diagrams for electron transfer (a) from excited pyrene monomer (Py) to conduction band of CCG and (b) from valence band of CCG to excited pyrene monomer in Py-2-CCG. The first oxidization and reduction potentials of the PP group were estimated by differential pulse voltammetry (DPV) measurements of 1-phenylpyrene (Py-ref).[S3b] The optical bandgap of the PP group was determined from the absorption edge of Py-ref. Fermi level of CCG is taken from a literature.[S11] The covalent functionalizations by the aryl radical reaction would induce optical bandgaps of ~0.4 eV in the CCG moieties.[S12] On a basis of the results of TA and absorption spectra under oxidation and reduction conditions, both processes in (a) and (b) can be ruled out for Py-2-CCG.

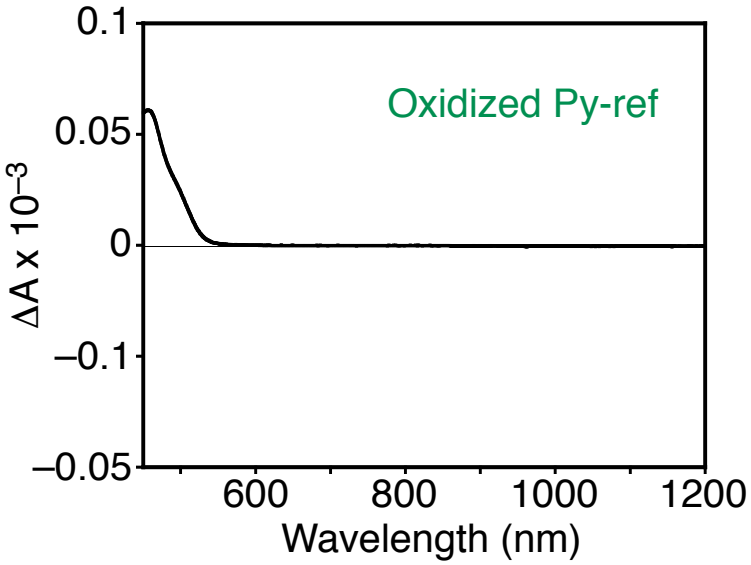

Fig. S11 Differential vis-NIR absorption (ΔA) spectrum of Py-ref electrochemically oxidized at +1.7 V vs. $Ag/AgNO_3$. The measurement was conducted in DMF using Bu_4NPF_6 (20 mM) as an electrolyte. The reference spectrum corresponds to the absorption spectrum recorded in the absence of an applied potential.

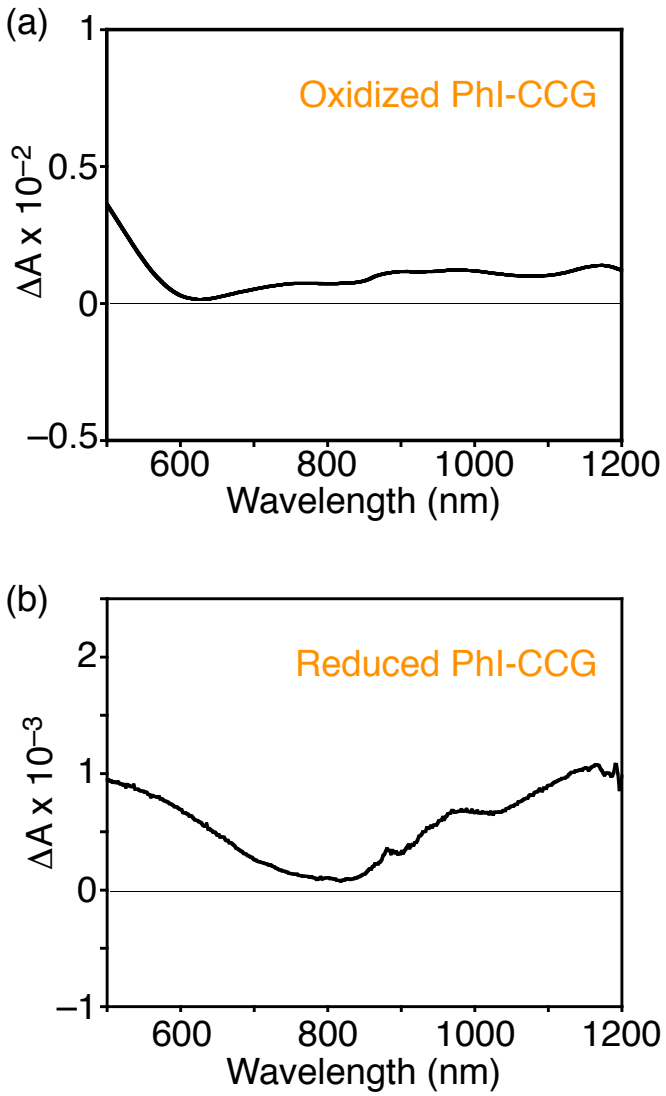

Fig. S12 Differential vis-NIR absorption (ΔA) spectra of PhI-CCG (a) chemically oxidized by adding an oxidant (0.036 μmol of $FeCl_3$) into PhI-CCG (0.144 mg) dispersion in DMF (3 mL) and (b) electrochemically reduced at –0.74 V vs. $Ag/AgNO_3$ in DMF using Bu_4NPF_6 (20 mM) as an electrolyte. The reference spectra correspond to the absorption spectra recorded in the absence of the chemical oxidant and the applied potential, respectively.

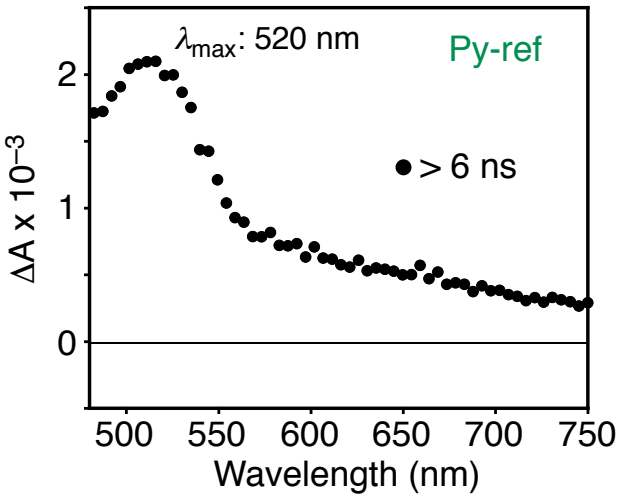

Fig. S13 Time-resolved transient absorption spectrum of Py-ref at > 6 ns in DMF. The excitation wavelength is 350 nm. This transient species is attributed to the first singlet excited state.[S3b,S13] The long decay lifetime (τ > 6 ns) is consistent with the emission lifetime of Py-ref (31.3 ns, Fig. S8a).

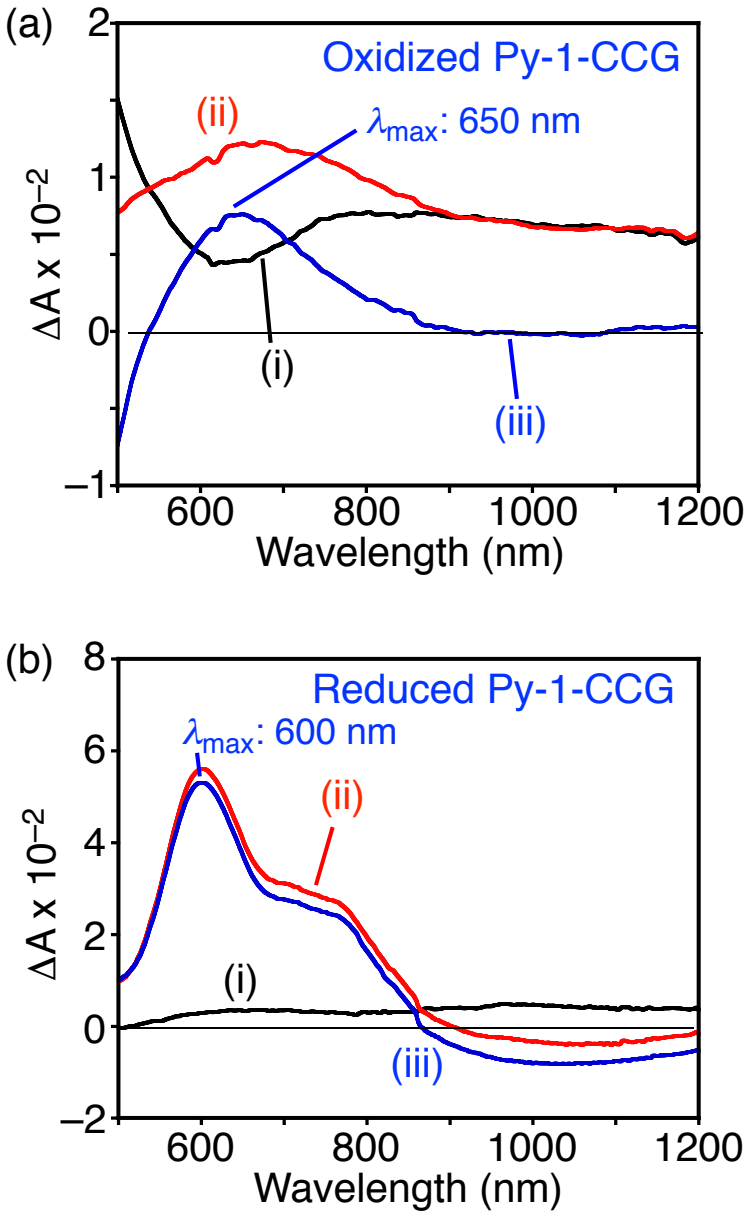

Fig. S14 (a) (i,ii) Differential vis-NIR absorption (ΔA) spectra of Py-1-CCG chemically oxidized by adding an oxidant ((i) 0.028 μmol and (ii) 0.14 μmol of $Cu(OSO_2CF_3)_2$) into Py-1-CCG (0.147 mg) dispersion in DMF (3 mL). The reference spectrum corresponds to the absorption spectrum recorded in the absence of the chemical oxidant. (iii) Differential spectrum of (ii) – (i). The spectra (i) and (iii) correspond to those for the oxidized CCG and the oxidized PP dimer, respectively. (b) Differential vis-NIR absorption (ΔA) spectra of Py-1-CCG electrochemically reduced at (i) –1.0 and (ii) –3.0 V vs. $Ag/AgNO_3$ in DMF using Bu_4NPF_6 (20 mM) as an electrolyte. The reference spectrum corresponds to the absorption spectrum recorded in the absence of the applied potential. (iii) Differential spectrum of (ii) – (i). The spectra (i) and (iii) correspond to those for the reduced CCG and the reduced PP dimer, respectively (See the Supporting discussion on absorption spectra in oxidized and reduced conditions).

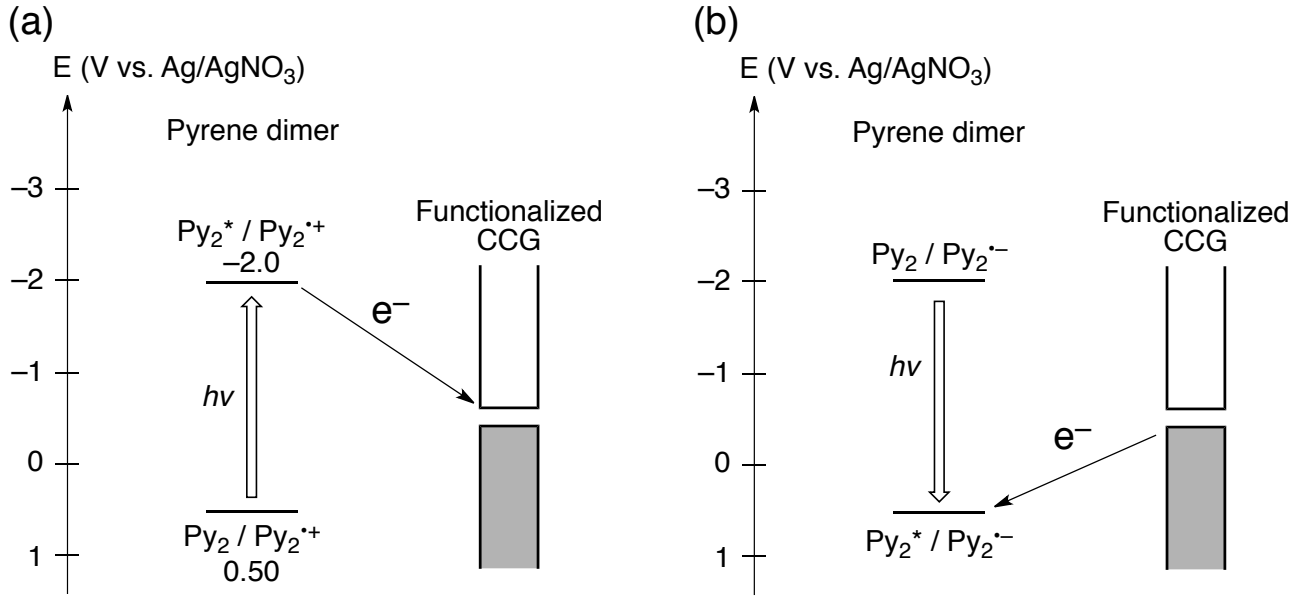

Fig. S15 Energy diagrams for electron transfer (a) from excited Pyrene dimer (Py_2) to conduction band of CCG and (b) from valence band of CCG to excited pyrene dimer in Py-1-CCG. The first oxidization potential of the pyrene dimer[S3b] and the Fermi level of CCG[S11] are taken from the literatures. The optical bandgap of the pyrene dimer was determined from the absorption edge of the pyrene dimer moiety in the spectrum of Py-1-CCG. The covalent functionalizations by the aryl radical reaction would induce optical bandgaps of ~0.4 eV in the CCG moieties.[S12] On a basis of the results of TA and absorption spectra under oxidation and reduction conditions, the process (b) can be ruled out for Py-1-CCG.

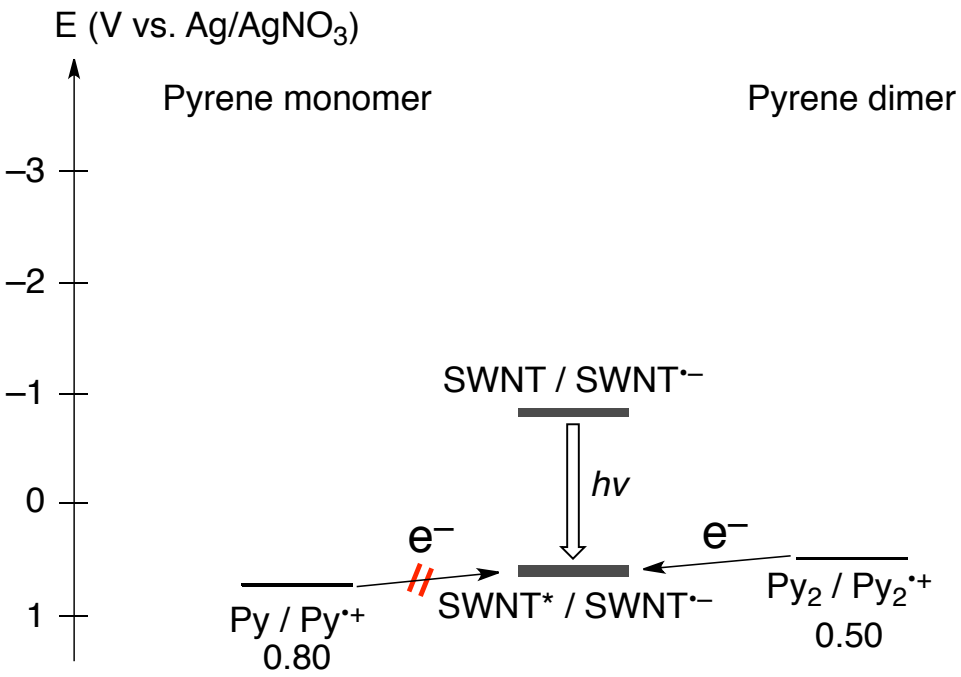

Fig. S16 Energy diagrams for electron transfer from the pyrene monomer (Py, left) and the pyrene dimer (Py_2, right) to the excited SWNT. The first oxidization potentials of pyrene dimer/monomer[S3b] and the first reduction potential and the optical bandgap of SWNT with chirality (6,5)[S14] are taken from the literatures.

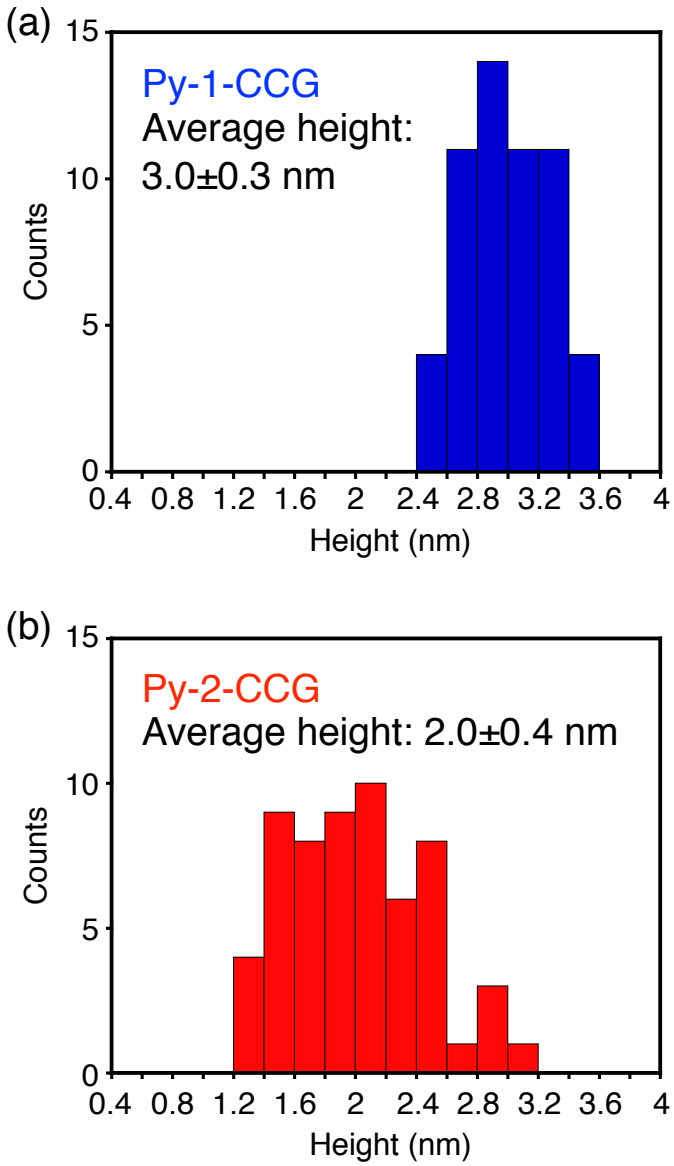

Fig. S17 Height distributions of exfoliated sheets of (a) Py-1-CCG and (b) Py-2-CCG estimated by AFM measurements. The samples were spin coated on mica from DMF dispersion. Cross-section profiles of (a) 55 and (b) 59 individual sheets of Py-1-CCG and Py-2-CCG, respectively, were analyzed.

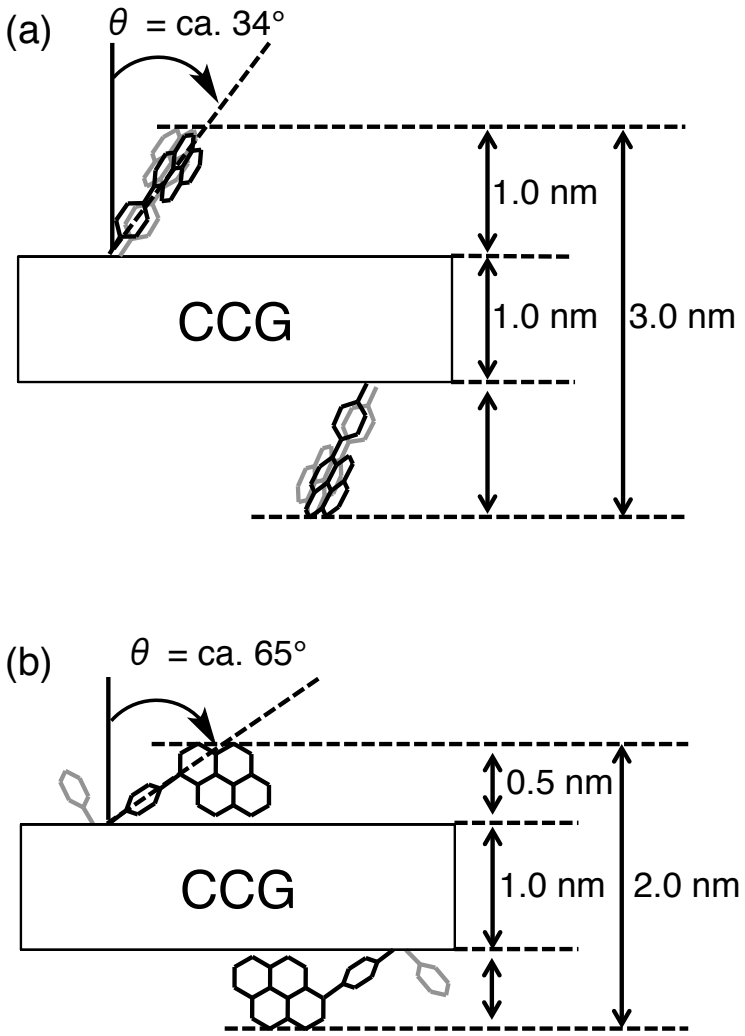

Fig. S18 Schematic structures of (a) Py-1-CCG and (b) Py-2-CCG.

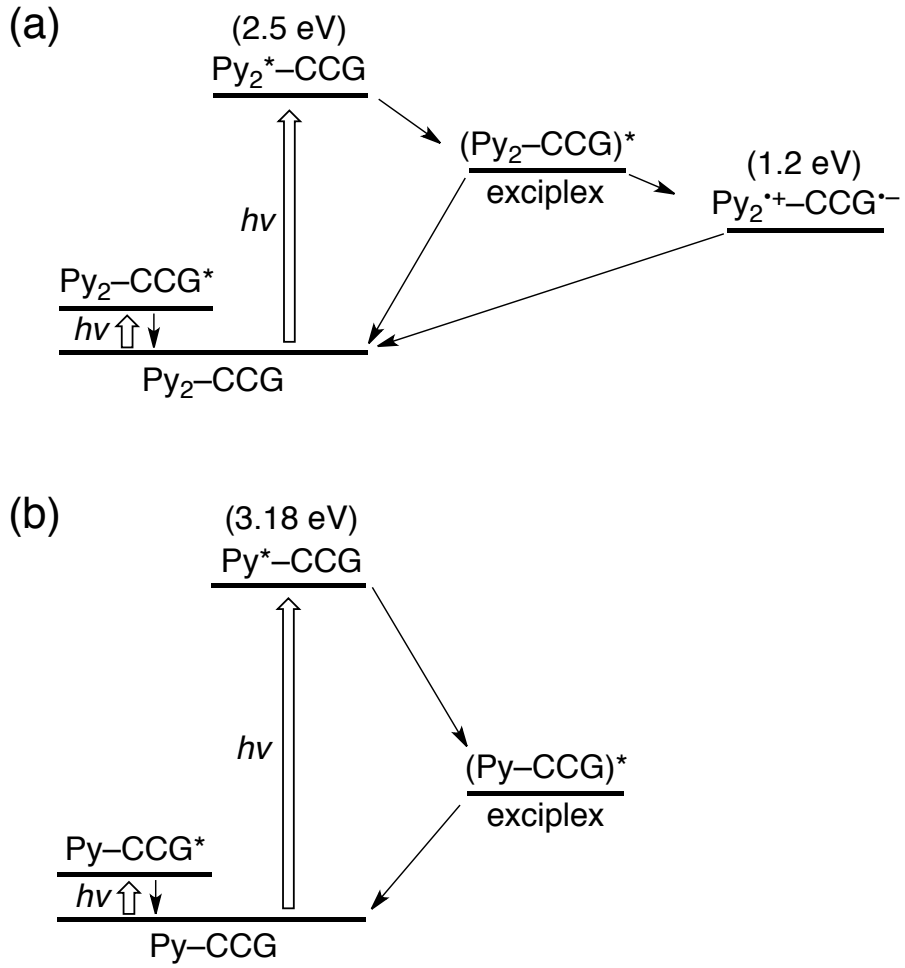

Fig. S19 Schematic relaxation pathways of (a) Py-1-CCG and (b) Py-2-CCG. The processes of EN or charge separation from the excited state of CCG moiety are ruled out in both of Py-1-CCG and Py-2-CCG due to the small bandgap of CCG.[S12] The excited CCG moiety rapidly relaxes to the ground state via vibrational processes.

References

[S1] (*a*) E. Maligaspe, N. V. Tkachenko, N. K. Subbaiyan, R. Chitta, M. E. Zandler, H. Lemmetyinen and F. D'Souza, *J. Phys. Chem. A*, 2009, **113**, 8478; (*b*) N. V. Tkachenko, L. Rantala, A. Y. Tauber, J. Helaja, P. H. Hynninen and H. Lemmetyinen, *J. Am. Chem. Soc.*, 1999, **121**, 9378; (*c*) V. Vehmanen, N. V. Tkachenko, H. Imahori, S. Fukuzumi and H. Lemmetyinen, *Spectrochim Acta A*, 2001, **57**, 2229; (*d*) M. Isosomppi, N. V. Tkachenko, A. Efimov and H. Lemmetyinen, *J. Phys. Chem. A*, 2005, **109**, 4881.

[S2] D. Sirbu, C. Turta, A. C. Benniston, F. Abou-Chahine, H. Lemmetyinen, N. V. Tkachenko, C. Wood and E. Gibson, *RSC Adv.*, 2014, **4**, 22733.

[S3] (*a*) S. Hagopian and L. A. Singer, *J. Am. Chem. Soc.*, 1985, **107**, 1874; (*b*) T. Umeyama, J. Baek, Y. Sato, K. Suenaga, F. Abou-Chahine, N. V. Tkachenko, H. Lemmetyinen and H. Imahori, *Nat. Commun.*, 2015, **6**, 7732.

[S4] J. N. Moorthy, P. Natarajan, P. Venkatakrishnan, D.-F. Huang and T. J. Chow, *Org. Lett.*, 2007, **9**, 5215.

[S5] T. Umeyama, J. Mihara, N. Tezuka, Y. Matano, K. Stranius, V. Chukharev, N. V. Tkachenko, H. Lemmetyinen, K. Noda, K. Matsushige, T. Shishido, Z. Liu, K. Hirose-Takai, K. Suenaga and H. Imahori, *Chem. Eur. J.*, 2012, **18**, 4250.

[S6] K. C. Stylianou, R. Heck, S. Y. Chong, J. Bacsa, J. T. A. Jones, Y. Z. Khimyak, D. Bradshaw and M. J. Rosseinsky, *J. Am. Chem. Soc.*, 2010, **132**, 4119.

[S7] T. Umeyama, M. Fujita, N. Tezuka, N. Kadota, Y. Matano, K. Yoshida, S. Isoda and H. Imahori, *J. Phys. Chem. C*, 2007, **111**, 11484.

[S8] K. C., C. Bikram, S. K. Das, K. Ohkubo, S. Fukuzumi and F. D'Souza, *Chem. Commun.*, 2012, **48**, 11859.

[S9] J. Daub, R. Engl, J. Kurzawa, S. E. Miller, S. Schneider, A. Stockmann and M. R. Wasielewski, *J. Phys. Chem. A*, 2001, **105**, 5655.

[S10] J. R. Lomeda, C. D. Doyle, D. V. Kosynkin, W.-F. Hwang and J. M. Tour, *J. Am. Chem. Soc.*, 2008, **130**, 16201.

[S11] (*a*) H. Hayashi, I. V. Lightcap, M. Tsujimoto, M. Takano, T. Umeyama, P. V. Kamat and H. Imahori, *J. Am. Chem. Soc.*, 2011, **133**, 7684; (*b*) T. Umeyama, D. Matano, J. Baek, S. Gupta, S. Ito, V. Subramanian and H. Imahori, *Chem. Lett.*, 2015, **44**, 1410.

[S12] (*a*) S. Niyogi, E. Bekyarova, M. E. Itkis, H. Zhang, K. Shepperd, J. Hick, M. Sprinkle, C. Berger, C. N. Lau, W. A. de Heer, E. H. Conrad and R. C. Haddon, *Nano Lett.*, 2010, **10**, 4061; (*b*) G. L. C. Paulus, Q. H. Wang and M. S. Strano, *Acc. Chem. Res.*, 2013, **46**, 160.

[S13] N. P. Gritsan, E. A. Pritchina, I. I. Barabanov, G. T. Burdzinski and M. S. Platz, *J. Phys. Chem. C*, 2009, **113**, 11579.

[S14] (*a*) Y. Hirana, G. Juhasz, Y. Miyauchi, S. Mouri, K. Matsuda and N. Nakashima, *Sci. Rep.*, 2013, **3**, 2959; (*b*) Y. Tanaka, Y. Hirana, Y. Niidome, K. Kato, S. Saito and N. Nakashima, *Angew. Chem. Int. Ed.*, 2009, **48**, 7655.